Enhancement of thermoelectric performance across the topological phase transition in dense lead selenide

Liu-Cheng Chen¹, Pei-Qi Chen², Wei-Jian Li¹, Qian Zhang^{3,4}, Viktor V. Struzhkin^{1,5}, Alexander F. Goncharov⁵, Zhifeng Ren⁴ & Xiao-Jia Chen¹

¹Center for High Pressure Science and Technology Advanced Research, Shanghai, 201203, China

²Massachusetts Institute of Technology, Cambridge, Massachusetts 02139, USA

³Department of Materials Science and Engineering, Harbin Institute of Technology, Shenzhen, Guangdong 518055, China

⁴Department of Physics and TcSUH, University of Houston, TX 77204, USA

⁵Geophysical Laboratory, Carnegie Institution of Washington, Washington, DC 20015, USA

To meet the world's current energy challenges of short supplies and dependence on polluting fossil fuels, alternative clean energy sources are in demand. Thermoelectric generators, which can generate electricity directly from waste heat with the advantages of reliability and compactness, are considered as potential devices for waste heat recovery. The thermoelectric performance is usually evaluated by a parameter known as the figure of merit zT. The maximum zT at room temperature has remained at around 1.0 for over 60 years. For practical technological applications, it is highly desired to break this barrier. Here, we study the pressure effects on zT by choosing a Cr-doped PbSe with a maximum zT of less than 1.0 at high temperature of about 700 K. By applying external pressure, we obtain the record

high zT value of \sim 1.7 at room temperature. A pressure-driven topological phase transition is found to account for such a huge enhancement. Experiments also support the appearance of a topological crystalline insulator after the transition. These findings point to a new direction for improving zT in the existing thermoelectric materials as well as the realization of the topological crystalline insulators from these materials just through compression.

Thermoelectric (TE) materials have demonstrated great potential in enabling the conversion between thermal and electrical energy, which is especially useful in the face of the current global energy crisis^{1–3}. The critical limitation for the TE materials studied so far is their relatively low conversion efficiency, which is determined by the thermoelectric figure of merit. The figure of merit is defined as $zT = S^2 \sigma T/\kappa$, where S is the Seebeck coefficient, σ is the electrical conductivity, T is the absolute temperature, and κ is the thermal conductivity. The interdependencies of S, σ , and κ complicate the efforts to improve zT. For a TE device with a Carnot efficiency of more than 15%, a TE material with an average $zT \geqslant 1.5$ should be used . Such high peak zT values have indeed been realized at high temperatures in many bulk materials^{4–10}. However, many technological applications require the operation of TE materials at room temperature. Only a few families have been reported to possess $zT \sim 1$ close to room temperature^{4,11}. This zT record remained unbroken for over 60 years¹².

Exploring the principle controlling zT enhancement and searching for new materials with efficient TE performance are the two key tasks in this research field. Doping and alloying have generally been used as methods to optimize the carrier concentration in order to enhance the elec-

trical transport properties¹⁻³. Nanostructuring can significantly reduce thermal conductivity due to the enhancement of boundary scattering⁴. This technique led to the discoveries of rather high peak $zT \sim 2.2$ in PbTe/SrTe and AgPb_mSbTe_{2+m}^{6,7}. Similarly, the zT enhancement was found in some nanoscale materials in their superparamagnetic states due to the considerable reduction of the thermal conductivity¹³. Meanwhile, some novel approaches and materials have been developed on the basis of unique band structure or lattice structure, such as the electronic density distortion⁸, and the band convergence effect⁹, as well as the existence of a charge density wave state 14 . The realization of high zT in liquid-like thermoelectrics 10 is thought to result from both the optimization of the electrical transport properties and the reduction of the thermal conductivity. Pressure as a fundamental thermodynamic variable can dramatically modify the crystal, electronic, and magnetic structure of a material without introducing impurities. The application of pressure has led to the significant improvement of the power factor ($PF = S^2\sigma$) in many thermoelectric materials ^{15,16}. With recent technique developments, all TE properties can now be measured at high pressures 17,18 . Large zT enhancement has been achieved upon compression 17,18 . It turns out that the same maximum zT value at high temperature in a material can be reached at room temperature solely by applying pressure 18 . Here we choose $Pb_{0.99}Cr_{0.01}Se$ as an example to show how pressure can be used to tune TE properties. This material has the highest TE efficiency among all of the n-type and p-type PbSe materials reported to date $^{19-26}$. We show that a room-temperature value of zT increases dramatically under pressure reaching 1.7 at pressure around 3 GPa. This is the record at the operating temperature of 300 K among all of the TE materials studied so far¹⁻³. Furthermore, we achieve a topological crystalline insulator (TCI) at higher pressures, which was theoretically

predicted in such a material class^{27–29}.

In order to establish the baseline for the TE properties of Pb_{0.99}Cr_{0.01}Se at high pressures, we began by measuring the electrical and thermal transport properties from 2 to 300 K at ambient pressure. The results are shown in Fig. S1 of the Supplementary Information (SI). The data at high temperatures were taken from earlier measurements of the same sample²⁶. Good agreement can be seen between the low and high temperature regimes. The minor deviations of the studied TE parameters near 300 K arise mainly from small systematic errors in the two experiments. Although PbSe has a very small direct band gap¹⁹, σ of Pb_{0.99}Cr_{0.01}Se decreases sharply upon cooling at low temperatures and then saturates with further decreasing temperature, exhibiting a semiconducting behaviour. In addition, the negative value of S continuously decreases with increasing temperature, indicating a n-type degenerate semiconducting character. The temperature dependence of κ has a typical λ shape – increasing sharply as T^{-3} and then decreasing as T^{-1} with increasing temperature after passing the maximum value. Generally, this typical behavior of κ is controlled by grain boundary scattering and three-phonon scattering via umklapp processes 1-3. The power factor PF is also shown in Fig. S1 of the SI. The maximum value of PF is about 30 μ W cm⁻¹K⁻² at 300 K. Such a maximum provides a good starting point for our study focusing on TE performance at 300 K.

Figures 1a and 1b show the temperature-dependent zT at ambient pressure and pressure-dependent zT at 300 K, respectively. As observed, the zT values at low temperatures agree well with another set of data at high temperatures (Fig. 1a), as a result of the parameters σ , S, κ , and

PF being self-consistent over the whole temperature range (Fig. S1 of the SI). The Cr-doped PbSe shares the same structure with its parent compound at ambient pressure (B1 phase, shown in the inset of Fig. 1a). With increasing temperature, zT monotonically increases until reaching the maximum value (less than 1) near 700 K and then decreases at higher temperatures. With increasing pressure, zT first monotonically increases until 2 GPa and then jumps up and reaches a maximum value of \sim 1.7 at about 2.8 GPa (Fig. 1b). It then continuously decreases until 4.5 GPa before finally maintaining a nearly constant value until near 6 GPa.

From the high-pressure X-ray diffraction data, we can find that all of the Bragg peaks of $Pb_{0.99}Cr_{0.01}Se$ shift monotonically to higher angles with increasing pressure, indicating the shrinkage of the lattice (Fig. S2 of the SI). New peaks emerge when pressure is increased to 5.5 GPa, indicating the phase transition from B1 to Pnma (Fig. S2 and Note 1 of the SI). The obtained lattice parameters of these two phases are shown in Fig. S2 of the SI. The two phases coexist in the pressure range from 5.5 to 8.5 GPa. The same behaviour is also detected from Raman scattering measurements (Fig. S3 and Note 2 of the SI). The obtained significant enhancement of the zT value is in the B1 phase.

The detailed results of the resistivity ρ of Pb_{0.99}Cr_{0.01}Se as a function of temperature for selected pressures are summarized in Fig. 2. As can be seen, the temperature-dependent ρ is strongly suppressed by increasing pressure up to 3.4 GPa and shows metallic behaviour. Upon further compression, ρ has a sudden increase and is characterized by a non-metallic feature at pressure of 4.2 GPa (Fig. 2a). The room-temperature electrical conductivity σ at various pressures was extracted

from the temperature dependences and the results are illustrated in Fig. 2b. Compared with the ambient pressure value, the room-temperature σ increases significantly with increasing pressure and reaches the maximum value ($\approx 44 \times 10^5 \ \mathrm{S} \ \mathrm{m}^{-1}$) at about 3.4 GPa. σ then drops sharply with further increasing pressure up to 4.5 GPa. Upon heavy compression to near 6 GPa, σ has only a small additional dip, which may be due to the appearance of the more stable Pnma structure (Fig. S2 of the SI). Our high-pressure resistivity data are similar to the previous reports for the undoped material 16. The sharp increase of σ between 2 and 3.5 GPa does not originate from a structural transition (Figs. S2 and S3 of the SI). The emergence of the sharply increased σ is likely controlled by the electronic structure, which is tuned by pressure. We assign the σ behaviour to the pressure-driven topological phase transition (TPT)^{30,31} as will be elaborated later based on other observations and calculations.

The high-pressure Seebeck coefficient S was determined based on the technique developed recently^{17,18}. The details are given in the Methods section and Fig. S4 of the SI. The pressure dependence of S for $Pb_{0.99}Cr_{0.01}Se$ at 300 K is summarized in Fig. 3a. The results are similar to previous reports on undoped $PbSe^{16}$. In the pressure range studied, all of the S values are negative, indicating the electron doping feature by introducing S. The absolute value of S decreases with increasing pressure until reaching a dip at around 3.8 GPa before climbing up at higher pressures. The asymmetrical form of S with external pressure is the typical feature expected in the vicinity of S and S is the derivative of the density of states at the Fermi level, it is strongly affected by S and S is the derivative of the density of the SI). Moreover, the TPT scenario also

offers a natural explanation for the observed bell shape of the pressure dependence of σ (Fig. 2). Here pressure serves as an external parameter that tunes the system.

By combining σ and S, one can obtain PF for $Pb_{0.99}Cr_{0.01}Se$ at high pressures. The results are shown in Fig. 3b. It can be seen that the PF value clearly increases with increasing pressure in the vicinity of P_c around 3 GPa, and then decreases rapidly after passing the maximum value of 210 μ W cm⁻¹ K⁻². This maximum PF is almost one order of magnitude higher than those through doping either by electrons^{20,21,24–26} or holes^{22,23}. The summary of the maximum value of the PF of the n-type PbSe materials at the corresponding temperature in the literature is given in Table S1 of the SI. The significant improvement of the PF under pressure is mainly attributed to the sharply increased σ values without a substantial reduction of S. Both the bell shape of σ and the asymmetrical form of S indicate the pressure-driven TPT. They together contribute to the bell shape of the PF.

To further understand the obtained electrical transport properties, we also performed high-pressure Hall effect measurements. The carrier mobility (μ) of the bulk material can be calculated from the measured Hall resistance and σ . The obtained μ and the carrier concentration n_H as a function of pressure for Pb_{0.99}Cr_{0.01}Se at 300 K are shown in Fig. S6 of the SI. The negative sign of n_H confirms the electron doping by Cr. At ambient pressure, n_H has a nearly optimal absolute value of $\approx 1 \times 10^{19}$ cm⁻³, indicting the excellent thermoelectric performance of this material even at ambient pressure. The absolute value of n_H increases monotonically with increasing pressure to 3×10^{19} cm⁻³ at 4.2 GPa. It then has a sudden decrease upon further compression (Fig. S6a of

the SI). However, the mobility μ exhibits a peak at around 3 GPa (Fig. S6b of the SI). Therefore, we attribute the significant increase of the PF value of $Pb_{0.99}Cr_{0.01}Se$ to TPT. These results show that applying pressure to drive a system across the TPT is indeed an efficient means to improve the PF of TE materials.

Band inversion in the bulk insulating electronic structure is the key requirement for the appearance of metallic surface states in TCIs with crystal symmetry²⁷. For the face-centered-cubic Brillouin zone (Fig. 4a), the (111) phane containing the high-symmetry points Γ , L, U, and X is chosen to show pressure-induced band inversion and TPT. The results are presented in Figs. 4b and 4c. The projected (001) surface containing $\bar{\Gamma}$, \bar{X} , and \bar{M} is chosen to show the formation of the surface states for TCI after the TPT (Fig. 4d). The calculated band structure for PbSe reveals pressure-driven band inversion (Fig. 4b and Fig. S7 of the SI). The band gap near the high symmetry point L in the Brillouin zone is found to narrow down upon compression and close at 2.6 GPa and then reopen afterward with an inversion between the conduction band and the valence band³². The TPT is accompanied by this inversion process (Fig. 4c). From the top view over the (111) plane, the small pockets represent available electronic states close to the top of the valence band. The pockets outside of the center hexagon are located at L point, and the pockets inside the hexagon are located at the Γ – U line. At ambient pressure, the center pocket is located at the Γ – L line. At 2.6 GPa, the center pocket located on the Γ – L lines disappears, which is a characteristic of the TPT. When the bulk bandgap reopens, the material enters a TCI state with the metallic feature from the surface but the insulating one from the bulk (Fig. 4d).

The linear magnetoresistance at low magnetic fields is a hallmark for topological insulators³³. We do detect such a feature when the material passes the TPT, e.q. the linear magnetoresistivity at pressure of 4.2 GPa and low temperature of 15 K. This differs to the nearly parabolic magnetic field dependence of the magnetoresistivity for pressures below P_c for the TPT (Fig. 4e). The linear magnetoresistivity provides the direct transport evidence for the experimental realization of the TCI state in this material. The cone shape of the magnetoresistivity vs. magnetic field is also observed for higher pressures far beyond the TPT (the case for 5.2 GPa in Fig. 4e). This behaviour probably results from a collective effect of the weak antilocalization of the surface bands and weak localization of the bulk bands in topological insulators³⁴. The enhanced weak localization effect from the bulk bands for pressures far beyond the TPT is due to the reopened bandgap as such higher pressures (Fig. 4b). These magnetoresistivity results are in excellent agreements with the pictures for the TPT and TCI as indicated in Figs. 4b-4d. This is further supported by the observed pressure-dependent behaviours of ρ and S, the maxima of the widths of two phonon modes and the minima of the difference of their energies (frequencies) (Figs. S3 and S5 of the SI). The experimental realization of the TCI state in Pb_{0.99}Cr_{0.01}Se solely through pressure^{28,29} is another central finding of this work.

For exploring thermoelectric performance, we carried out high-pressure κ measurements by using our newly developed technique^{17,18}. The details are given in the Methods section and Note 4 together with Figs. S8 and S9 of the SI. The obtained κ for Pb_{0.99}Cr_{0.01}Se increases by approximately a factor of four with the application of pressure up to 4.8 GPa (Fig. 5). The obtained large Grüneisen parameters are a good indicator for the good heat conduction in this material in

the B1 phase (Note 5 of the SI). When the Pnma phase is evident, κ jumps up to a larger value. In the B1 phase, the obtained pressure dependences of σ and the full width at half maximum of the phonon mode can be used to provide the quantitative estimation of the electronic and lattice contributions to κ (Note 6 of the SI). As can be seen from Fig. S10 of the SI, the lattice component of κ behaves almost the same as the total κ except for the slight decline in the vicinity of P_c for the TPT. Meanwhile, the electronic component of κ exhibits an asymmetrical shape with a maximum at \sim 3.7 GPa. As a results, both the lattice and electrons jointly conduct heat at high pressures. The high-pressure thermal conductivity is also strongly affected by the TPT in this material. The pressure-dependent zT of Pb_{0.99}Cr_{0.01}Se at 300 K was thus determined for each pressure based on the obtained σ , S, and κ values (Fig. 1b). It is apparent that the pressure-induced increase of κ is not a favorable factor for zT. The significant enhancement of zT with pressure results from the increase of PF through the large improvement of σ due to the pressure-driven TPT.

We found an enhanced room-temperature zT in $Pb_{0.99}Cr_{0.01}Se$ at P_c of around 3 GPa, followed by the entrance to a TCI phase. A pressure-driven TPT is believed to account for such an enhancement. The supported σ and S data (Fig. S11 of the SI) and Raman spectra (Fig. S3 of the SI) are reproducible. Although different experimental runs could give scattered values for PF and thus zT, the pressure-dependent zT with maximum values above 1 at certain critical pressures can be firmly established for this material even when averaging all of the available data (Fig. S11 of the SI). The present study thus offers a new direction to further improve the thermoelectric performance of existing thermoelectric materials simply through lattice compression or other equivalent methods that can be used to tune the material to the TPT conditions.

Instead of reaching the optimal conditions for the enhances zT by compression, one can explore a possibility of chemical doping that would shrink the lattice. An excellent example along this direction was the discovery of the first cuprate superconductor with a critical temperature above liquid nitrogen temperature, which was triggered by the observed strong pressure effect in the La-Ba-Cu-O system³⁵. Whether similar enhancement in the zT of thermoelectric materials can be realized through lattice shrinkage at ambient pressure remains to be seen and deserves further study. However, this idea has been realized already by creating TCI states in $Pb_{1-x}Sn_xSe^{36}$ and $Pb_{1-x}Sn_xTe^{37}$. Doping Sn in both ternary alloys to reduce crystal volume is thus expected to result in excellent thermoelectric performance due to the gap closure and occurrence of TPT at certain temperatures^{36–38}.

- 1. Chen, G., Dresselhaus, M. S., Dresselhaus, G., Fleurial, J. P. & Cailla, T. Recent developments in thermoelectric materials. *Int. Mater. Rev.* **48**, 45-66 (2003).
- 2. Snyder, G. J. & Toberer, E. S. Complex thermoelectric materials. *Nat. Mater.* **7**, 105-144 (2008).
- 3. Ren, Z. F., Lan, Y. C. & Zhang, Q. Y. Advanced thermoelectrics: Materials, contacts, devices, and system. CRC Press, 2017.
- 4. Poudel, B. *et al.* High-thermoelectric performance of nanostructured bismuth antimony telluride bulk alloys. *Science* **320**, 634-638 (2008).
- 5. Pei, Y. Z., Heinz, N. A., LaLonde, A. & Snyder, G. J. Combination of large nanostructures and complex band structure for high performance thermoelectric lead telluride. *Energy Env*-

- iron. Sci. 4, 3640-3645 (2011).
- 6. Biswas, K. *et al.* High-performance bulk thermoelectrics with all-scale hierarchical architectures. *Nature* **489**, 414-418 (2012).
- 7. Hsu, K. F. *et al.* Cubic AgPb_mSbTe_{2+m}: Bulk thermoelectric materials with high figure of merit. *Science* **303**, 818-821 (2004).
- 8. Heremans, J. P. *et al.* Enhancement of thermoelectric efficiency in PbTe by distortion of the electronic density of states. *Science* **321**, 554-557 (2008).
- 9. Pei, Y. Z., Shi, X., LaLonde, A., Wang, H., Chen, L., & Snyder, G. J. Convergence of electronic bands for high performance bulk thermoelectrics. *Nature* **473**, 66-69 (2011).
- 10. Liu, H. et al. Copper ion liquid-like thermoelectrics. Nat. Mater. 11, 422-425 (2012).
- 11. Zhu, T. J. *et al.* Hot deformation induced bulk nanostructuring of unidirectionally grown *p*-type (Bi,Sb)₂Te₃ thermoelectric materials. *J. Mater. Chem. A*, **1**, 11589-11594 (2013).
- 12. Wright, D. A. Thermoelectric properties of bismuth telluride and its alloys. *Nature* **181**, 834-834 (1958).
- 13. Zhao, W. *et al.* Superparamagnetic enhancement of thermoelectric performance. *Nature* **549**, 247-251 (2017).
- 14. Rhyee, J. S. *et al*. Peierls distortion as a route to high thermoelectric performance in $In_4Se_{3-\delta}$ crystals. *Nature* **459**, 965-968 (2009).

- Polvani, D. A., Meng, J. F., Chandra Shekar, N. V., Sharp, J. and Badding, J. V. Large Improvement in thermoelectric properties in pressure-tuned p-type Sb_{1.5}Bi_{0.5}Te₃. Chem. Mater.
 13, 2068-2071 (2001).
- 16. Shchennikov, V. V., Ovsyannikov, S. V. & Derevskov, A.Y. Thermopower of lead chalcogenides at high pressures. *Phys. Solid State* **44**, 1845-1849 (2002).
- 17. Yu, H. *et al.* Impressive enhancement of thermoelectric performance in CuInTe₂ upon compression. *Mater. Today Phys.* **5**, 1-5 (2018).
- 18. Chen, L. C. *et al.* Pressure-induced enhancement of thermoelectric performance in palladium sulfide. *Mater. Today Phys.* **5**, 64-71 (2018).
- 19. Parker, D. & Singh, D. J. High-temperature thermoelectric performance of heavily doped PbSe. *Phys. Rev. B* **82**, 035204 (2010).
- 20. Androulakis, J. *et al.* High-temperature thermoelectric properties of *n*-type PbSe doped with Ga, In, and Pb. *Phys. Rev. B* **83**, 195209 (2011).
- 21. Lee, Y. *et al.* Contrasting role of antimony and bismuth dopants on the thermoelectric performance of lead selenide. *Nat. Commun.* **5**, 3640 (2014).
- 22. Wang, H., Pei, Y. Z., LaLonde, A. D., & Snyder, G. J. Heavily doped *p*-type PbSe with high thermoelectric performance: An alternative for PbTe. *Adv. Mater.* **23**, 1366-1370 (2011).
- 23. Wang, H., Gibbs, Z. M., Takagiwa, Y. & Snyder, G. J. Tuning bands of PbSe for better thermoelectric efficiency. *Energy Environ. Sci.* **7**, 804-811 (2014).

- 24. Zhang, Q. *et al.* Study of the thermoelectric properties of lead selenide doped with boron, gallium, indium, or thallium. *J. Am. Chem. Soc.* **134**, 17731-17738 (2012).
- 25. Zhang, Q. Y. *et al.* Enhancement of thermoelectric figure-of-merit by resonant states of aluminium doping in lead selenide. *Energy Environ. Sci.* **5**, 5246-5251 (2012).
- 26. Zhang, Q. *et al.* Enhancement of thermoelectric performance of *n*-type PbSe by Cr doping with optimized carrier concentration. *Adv. Energy Mater.* **5**, 1401977 (2015).
- 27. Fu, L. Topological crystalline insulators. *Phys. Rev. Lett.* **106**, 106802 (2011).
- 28. Hsieh, T. H. *et al.* Topological crystalline insulators in the SnTe material class. *Nat. Commun.* **3**, 982 (2012).
- 29. Barone, P. *et al.* Pressure-induced topological phase transitions in rocksalt chalcogenides. *Phys. Rev. B* **88**, 045207 (2013).
- 30. Abrikosov, A. A. Fundamentals of the theory of metals, North-Holland, Amsterdam, 1988.
- 31. Blanter, Ya. M., Kaganov, M. I., Pantsulaya, A. V. & Varlamov, A. A. The theory of electronic topological transitions. *Phys. Rep.* **245**, 159-257 (1994).
- 32. Svane, A. *et al.* Quasiparticle self-consistent *GW* calculations for PbS, PbSe, and PbTe: Band structure and pressure coefficients. *Phys. Rev. B* **81**, 245120 (2010).
- 33. Qu, D. X., Hor, Y. S., Xiong, J., Cava, R. J. & Ong, N. P. Quantum oscillations and Hall anomaly of surface states in the topological insulator Bi₂Te₃. *Science* **329**, 821-824 (2010).

- 34. Lu, H. Z. & Shen, S. Q. Weak localization of bulk channels in topological insulator thin films. *Phys. Rev. B* **84**, 125134 (2011).
- 35. Wu, M. K. *et al.* Superconductivity at 93 K in a new mixed-phase Y-Ba-Cu-O compound system at ambient pressure. *Phys. Rev. Lett.* **58**, 908-910 (1987).
- 36. Dziawa, P. *et al.* Topological crystalline insulator states in $Pb_{1-x}Sn_xSe$. *Nat. Mater.* **11**, 1023-1027 (2012).
- 37. Xu, S. Y. *et al.* Obervation of a topological crystalline insulator phase and topological phase transition in $Pb_{1-x}Sn_xTe$. *Nat. Commun.* **3**, 1192 (2012).
- 38. Dimmock, J. O., Melngailis, I. & Strauss, A. J. Band structure and laser action in $Pb_xSn_{1-x}Te$. *Phys. Rev. Lett.* **16**, 1193-1196 (1966).

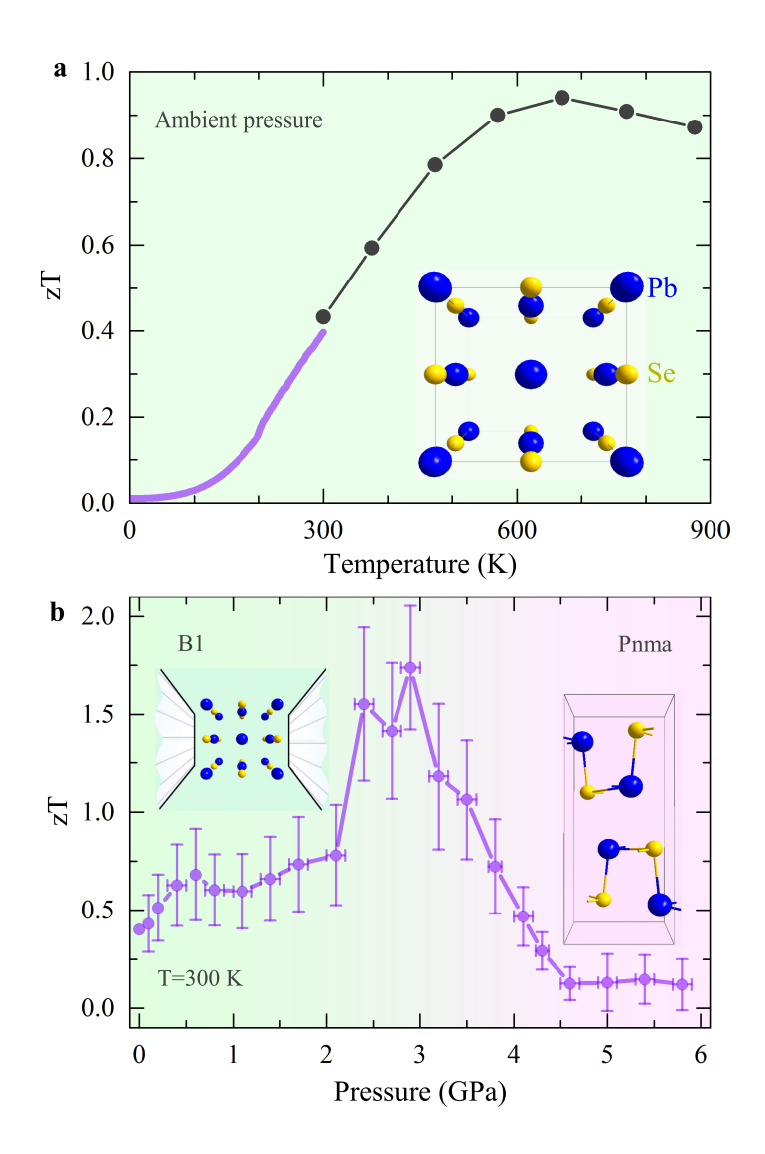


Figure 1 | The dimensionless figure of merit zT of $Pb_{0.99}Cr_{0.01}Se$. a, Temperature dependence of zT at ambient pressure. The zT values at low temperatures were obtained by using PPMS, and the data at high temperatures were taken from the earlier study on the same sample²⁶. The inset illustrates the crystal structure of the sample in the B1 phase. b, Pressure-dependent zT at 300 K. The errors for zT are given for the uncertainties in the measurements of the resistivity, Seebeck coefficient, and thermal conductivity. The structures for the B1 and Pnma phases are shown in the insets for the low-pressure and high-pressure regions, respectively.

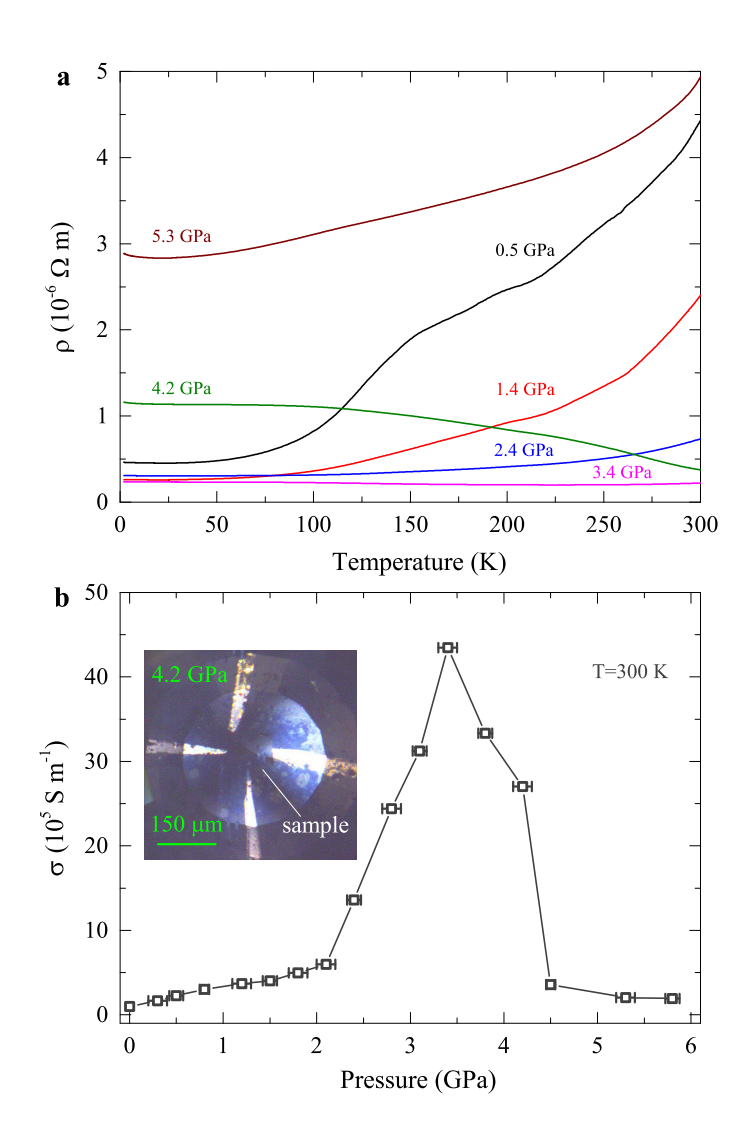


Figure 2 | The electrical resistivity and conductivity of $Pb_{0.99}Cr_{0.01}Se$ at high pressures. a, Temperature dependence of the resistivity ρ at various pressures up to 5.3 GPa. b, Pressure dependence of the electrical conductivity σ at 300 K. The inset shows the geometry of the electrical transport measurements at pressure of 4.2 GPa. Four Pt wires were used to attach the sample.

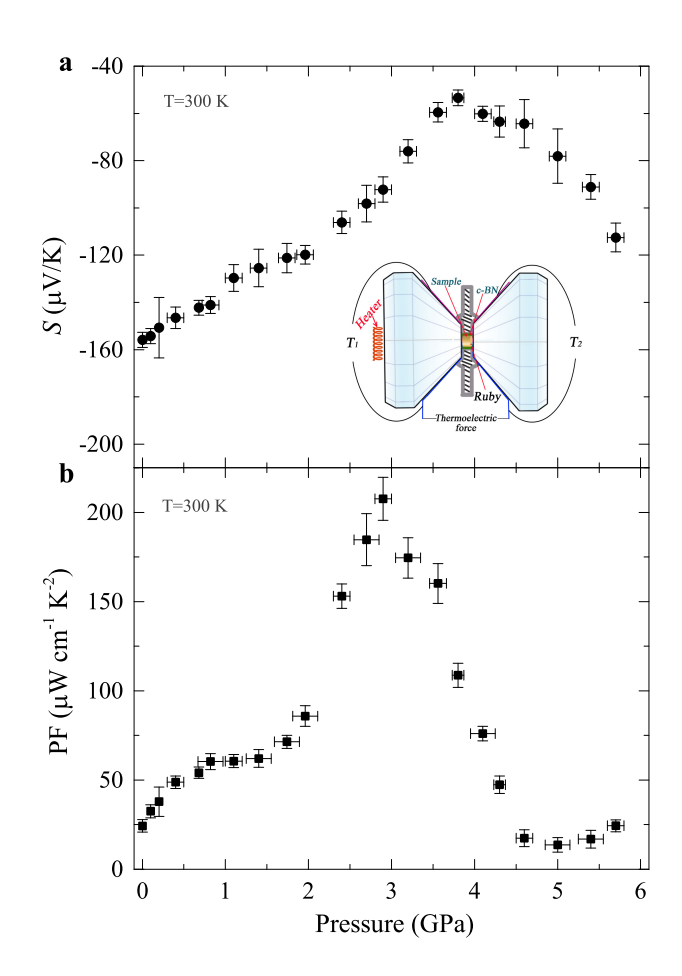


Figure 3 | The Seebeck coefficient and power factor of $Pb_{0.99}Cr_{0.01}Se$ at high pressures. a, Pressure dependence of the Seebeck coefficient S at 300 K. The insert shows the diagram of Seebeck coefficient measurements under pressure. The temperature gradient ($\Delta T = T1 - T2$) between the two sides of the sample is generated by an external heater attached to one side of the diamond. The ΔT is measured by two separate W-Ta thin thermocouples. At the same time, the thermoelectric voltage (ΔV) along the temperature gradient is measured by using the same thermocouple material. The sample was placed in the chamber, which was surrounded by cBN as insulating layers. Ruby was used to determine the pressure. b, Pressure dependence of the power factor PF at 300 K.

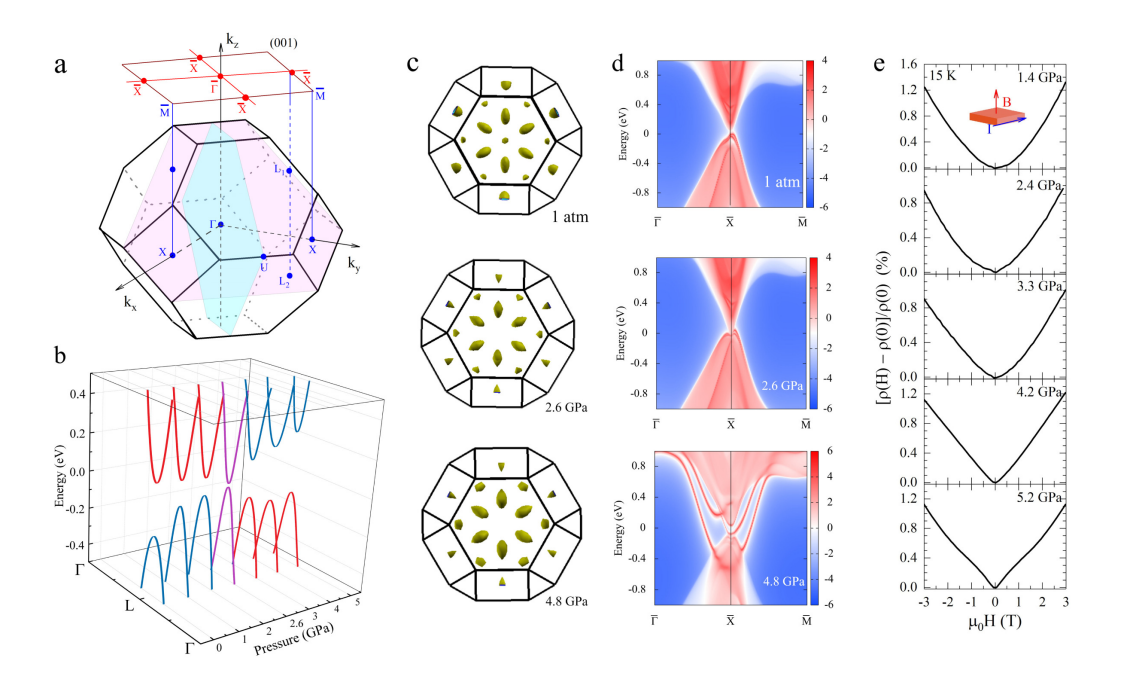


Figure 4 | Band structure and topological crystalline insulator state in $Pb_{0.99}Cr_{0.01}Se$ under pressure. a, The face-centered-cubic Brillouin zone. The colour (111) phane containing the high-symmetry points Γ, L, U, and X is chosen to show pressure-induced band inversion and TPT. The projection onto the (001) surface containing $\bar{\Gamma}$, \bar{X} , and \bar{M} is used to show the formation of the surface states for TCI after the TPT. b, Evolution of the band gap near the high symmetry point L for PbSe with pressure. The application of pressure leads to the band shrinkage, closure to nearly zero, and reopening with the band inversion at 2.6 GPa. c, Top view over the (111) plane at selected pressures to show the TPT character. The small pockets represent available electronic states close to the top of the valence band. The pockets outside of the center hexagon are located at L point, and the pockets inside the hexagon are located at the Γ – U line. d, Energy and momentum dispersion with the local density of states on the (001) surface at ambient pressure, 2.6 GPa, and 4.8 GPa (from the top to bottom). The surface states can be observed around the \bar{X} point with the reopened band gap for the bulk. A nontrivial TCI phase is formed after passing 2.6 GPa. e,

The magnetoresistivity $[\rho(H) - \rho(0)]/\rho(0)$ taken at temperature of 15 K for selected pressures as a function of the magnetic field H. The directions for the applied magnetic field and current on the sample are shown in the inset.

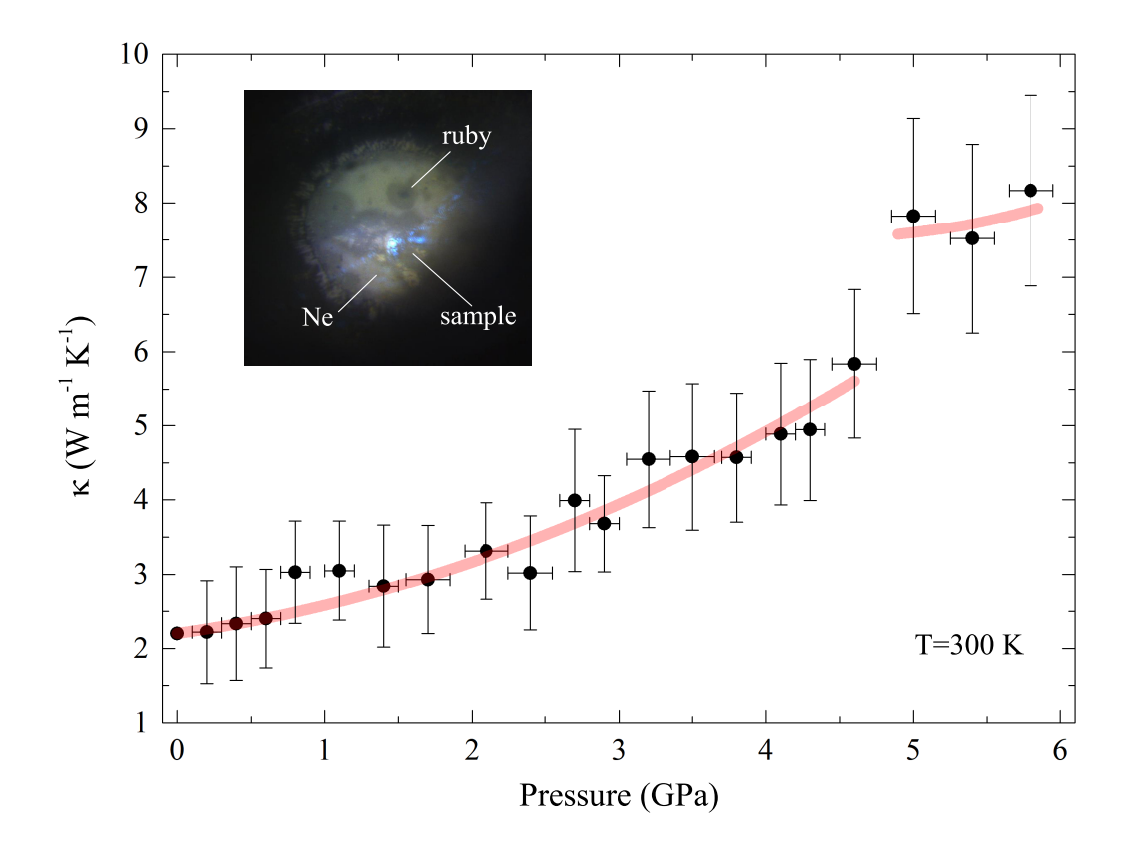


Figure 5 | The thermal conductivity of $Pb_{0.99}Cr_{0.01}Se$ at high pressures. The values of κ were obtained at each pressure of interest and at 300 K. The lines are the guides for the eye. This discontinuity of the data points and the curves indicates the structural transition. The inset shows the microscopic photograph for the measurements of the thermal conductivity under pressure. The ruby near the sample was used to determine pressure. Neon was loaded to serve as the pressure-transmitting medium. The details for the measurements are given in the SI.